Modeling of thin-film solar thermoelectric generators

Modeling of Thin-Film Solar Thermoelectric Generators

L. A. Weinstein, K. McEnaney, G. Chen*

Mechanical Engineering Department

Massachusetts Institute of Technology

Cambridge, MA 02139

Recent advances in solar thermoelectric generator (STEG) performance have raised their prospect as a potential technology to convert solar energy into electricity. This paper presents an analysis of thin-film STEGs. Properties and geometries of the devices are lumped into two parameters which are optimized to guide device design. The predicted efficiencies of thin-film STEGs are comparable to those of existing STEG configurations built on bulk materials.

I. INTRODUCTION

At present, the majority of solar energy harvesting to generate electricity has been via photovoltaic solar cells, or concentrated solar-thermal plants which run a traditional power cycle. An option that remains largely unpursued is the use of solar thermoelectric generators (STEGs)[1,2]. Thermoelectric materials develop a voltage gradient when a temperature gradient is applied[3]. For STEGs, a temperature gradient is achieved through the use of a solar absorber and a heat sink, allowing electricity to be generated from sunlight[1]. While the concept of a STEG is over one hundred years old[1], previous studies on STEGs[2,4-6] have shown poor results until recent developments that make use of a vacuum enclosure to reduce convective heat losses, selective surfaces for solar absorption and nanostructured thermoelectric

* Corresponding author, email: gchen2@mit.edu

materials[7]. Even higher efficiencies may be achieved via materials improvements and through the integration of optical concentration[8-11].

The recent demonstration by Kraemer et al. was based on bulk thermoelectric materials[7]. Unlike the conventional application of thermoelectric conversion of heat into electricity that requires physical contacts between the heat source and the thermoelectric generator, solar photons do not exert much force on the STEG. This leads to the possibility that thin-film thermoelectric materials, which have seen some progress in the past[12-14] can be used in STEGs. This would seem reasonable, as thin-film thermopile infrared detectors are commercially available[15,16] and thin-film photovoltaic devices have seen commercial success[17]. Previous studies have considered thin-film thermoelectric coolers and generators[18-20]. A recent study has investigated thin-film STEGs, however the performance found was significantly lower than bulk material STEG performance[21]. Thin-film STEGs operate at higher temperatures than thermopiles, and have special considerations regarding the area occupied by the thermoelectric legs and the heat sink.

This paper presents a modeling study on the performance of thin-film STEGs. In the next section, the device geometry is described and models with progressive sophistication are presented, starting from an isothermal absorber, followed by a model considering the temperature non-uniformity in the absorber, and numerical simulation including other non-idealities. Two key lumped parameters are derived which allow general discussion of the efficiency of thin-film STEGs of different geometries. In section III, results based on typical materials properties are discussed. It is found that thin-film STEGs can have similar performance as bulk materials-based STEGs.

II. Model

Figures 1(a) and 1(b) show schematics for the planar thin-film STEG being investigated. Solar insolation heats up the solar absorber and the hot side of the thermoelectric generator, and the surroundings keep the

cold side of the thermoelectric generator cool so that a temperature gradient is developed. In this configuration the solar absorber, thermoelectric legs and heat sink all lie in the same plane (with p-type legs on the left and n-type legs on the right). Benefits of this configuration are the potential for easier manufacturing and reduced material costs, as microfabrication techniques could allow for batch processing as well as extremely low material usage. The main disadvantage of this design is that intercepted sunlight is incident on the thermoelectric material and the heat sink, in addition to the solar absorber. Another disadvantage is that electrical current flows through the solar absorber, leading to resistance losses, although this can be avoided by placing p-n TE pairs on each side of the absorber. In this study, we will focus on the device configuration in Fig.1 and investigate the performance of this configuration for comparison to that of existing designs.

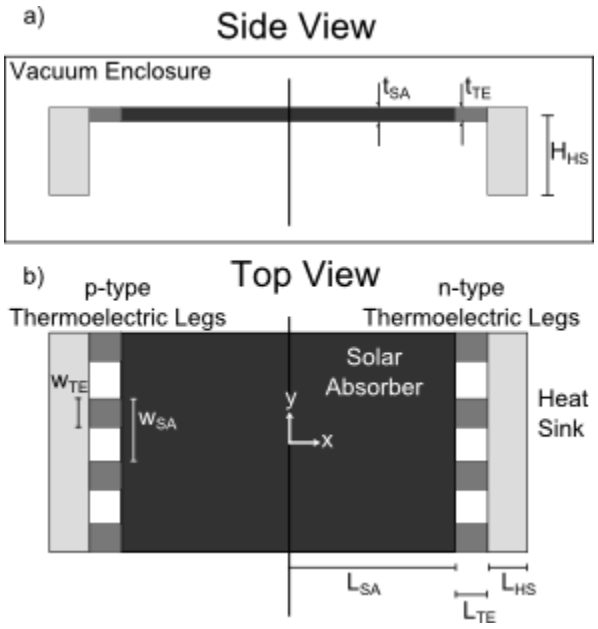

Figure 1a) side view and b) top view of thin-film STEG geometry, with relevant lengths labeled

Approximations used throughout the entirety of the paper are:

- The dimensionless thermoelectric figure of merit ZT_M is assumed constant,
- All other properties (e.g. absorber emissivity, absorptivity, conductivity, etc.) are assumed to be temperature independent,

- The far end of the heat sink is always maintained at ambient temperature,
- While in reality n and p-type thermoelectric materials have different properties, here they are assumed to be identical except for the sign of the Seebeck coefficient. This allows for symmetry across the midplane of the STEG, so that one half can be analyzed and the results will match those of the full device.
- All convective losses from the solar absorber are ignored, as they are assumed to be negligibly small due to the device being in an evacuated enclosure.

For the majority of this study the device is treated as one-dimensional, in the sense that temperature variations are only considered in the *x*-direction for the solar absorber. The validity of this approximation is verified in later sections. It should also be noted that the 1-D nature of the analysis leads to some areas being better represented by lengths. In these situations it can be assumed that the area in question is the length noted multiplied by a unit length in the *y*-direction.

We will first discuss the thin-film STEG performance under the ideal case, for which the absorber is treated as isothermal with no radiative losses from the TE legs, no electrical resistance in the solar absorber, and no plan area (area in the x-y plane) dedicated to the heat sink. This ideal case will provide an upper limit for the device efficiency. Following this, temperature variation in the absorber will be considered based on a differential analysis of the absorber. The bulk of the paper is based on a 1-D approximation. Additionally, brief treatments on the effects of manufacturing limitations, heat sink plan area, radiative losses from the TE legs, electrical resistance in the solar absorber, and 2-D temperature distributions in the absorber will be provided. We show that with proper design, thin-film STEGs can achieve similar performance as STEGs using bulk materials.

The operation of the thermoelectric elements is given by the following equations[3]:

$$Q_H = T_H SI + \frac{\Delta T}{R_T} - \frac{I^2 R_E}{2} \quad (1)$$

$$R_T = \frac{L_{TE}}{k_{TE} t_{TE} PF} \quad (2)$$

$$R_E = \frac{L_{TE}}{\sigma_e t_{TE} PF} \quad (3)$$

Q_H is the heat flowing through the thermoelectric elements, which is the sum of heat flow from the Peltier effect (the first term on the right hand side (RHS) of Eq. (1)) and Fourier conduction (the second term on the RHS) less half the heat generated in the elements from Joule heating (the third term on the RHS). T_H is the hot side temperature, ΔT is the temperature drop across the thermoelectric, S is the Seebeck coefficient of the TE element, and I is the electrical current through the TE element. R_T and R_E are the thermal and electrical resistances per unit depth of the TE leg respectively. L_{TE} is the length of the thermoelectric element, t_{TE} is the thickness, and PF is the packing fraction, or the proportion of total space in the y direction occupied by thermoelectric legs. k_{TE} is the thermal conductivity of the TE and σ_e is its electrical conductivity.

For STEGs, operation at maximum power generation corresponds to operation at maximum efficiency since a flux (incident solar radiation), not a heat reservoir, is this hot-side boundary condition[22]. The load matching condition to achieve maximum efficiency in STEGs is $R_L/R_E = \sqrt{1 + ZT_M}$ and accordingly this load matching condition is used for the entirety of the analysis[22], where Z is the thermoelectric figure of merit $S^2\sigma_e/k_{TE}$ and T_M is the mean TE temperature. Efficiency is given as simply the ratio of electrical power generated to solar radiation incident on the device:

$$\eta = \frac{P}{G(L_{SA} + L_{TE} + L_{HS})} \quad (4)$$

with G being solar insolation. It can also be shown that efficiency can be found as a product of three sub efficiencies:

$$\eta = \eta_{geom}\eta_{ot}\eta_{te} \tag{5}$$

$$\eta_{geom} = \frac{L_{SA}}{L_{SA} + L_{TE} + L_{HS}} \tag{6}$$

$$\eta_{ot} = \frac{Q_H}{L_{SA}G} \tag{7}$$

$$\eta_{te} = \frac{(T_H - T_C)}{T_H}\frac{\sqrt{1+ZT_M} - 1}{\sqrt{1+ZT_M} + T_C/T_H} \tag{8}$$

η_{geom} is a geometric efficiency which arises from light not striking the solar absorber being ignored, as the non-absorber plan area should be small and has not been optimized for absorbing sunlight. η_{ot} is the opto-thermal efficiency, which is the ratio of heat flow into the thermoelectric leg compared to sunlight intercepted by the absorber. Finally, η_{te} is the TE leg efficiency, which is simply the efficiency of a thermoelectric generator operating between a hot and cold temperature[3]. The inclusion of η_{geom} is what differentiates planar STEG performance from previous designs[22].

A. Isothermal absorber

In the simplest and most ideal model for the planar STEG the solar absorber is isothermal (equivalent to having infinite thermal conductivity), the thermoelectric legs are insulated except at the junctions (no radiative losses) the solar absorber is treated as having infinite electrical conductivity (no Joule heating in the absorber) and the cold side of the TE legs are assumed to be at T_C without the use of any device plan area for a heat sink ($L_{HS} = 0$). In this model, hot side temperature can be found from a steady-state energy balance in the solar absorber:

$$L_{SA}G\tau\alpha - L_{SA}\epsilon'\sigma\left(T_H^4 - T_C^4\right) - Q_H = 0 \tag{9}$$

with ε' being effective emissivity (emissivity with both front and backside losses considered). Here absorbed solar insolation (the first term on the left hand side (LHS)) must match radiation losses (the second term on the LHS) and heat flow through the thermoelectric legs Q_H. With device parameters and geometry set, Eqs. (1) and (9) are sufficient to find T_H, which then yields ΔT and therefore power and efficiency.

Using this equation, η_{ot} can be found as a simple function of hot side temperature[22]:

$$\eta_{ot} = \tau\alpha - \frac{\epsilon'\sigma(T_H^4 - T_C^4)}{G} \tag{10}$$

while the other efficiencies remain simple to calculate with a given geometry and hot side temperature. In practice, the hot side temperature is set by modifying device geometry.

B. 1-D Absorber temperature distribution

The previous analysis does not consider that radiative losses along the absorber will influence the temperature profile. This section considers a one-dimensional temperature distribution that arises in the absorber from radiative losses and finite absorber conduction. This reduces performance, as the TE elements see a reduced T_H and therefore a reduced ΔT. In reality there will also be radiative losses from the TE legs, however this is ignored now because the TE leg area should be small enough as to render those losses negligible, and this would introduce unnecessary complications into the modeling. Thus only radiative losses from the absorber are considered. Joule heating in the absorber is still ignored in this section, as we expect it to be negligible due to the absorber likely being composed of a highly electrically conductive metal (e.g. copper).

The temperature distribution in the absorber can be described by

$$\frac{d^2T}{dx^2} = \frac{\sigma\epsilon'(T^4 - T_C^4) - G\tau\alpha}{k_{SA}t_{SA}} \tag{11}$$

which is derived by taking a differential element of the absorber. The boundary condition for this differential equation at x = 0 (assigned to the center of the absorber) is no temperature gradient, which arises from symmetry. The boundary condition at the far end is that the heat flow out of the absorber

$$Q_H = -k_{SA}t_{SA}\frac{dT}{dx}\Big|_{L_{SA}} \tag{12}$$

must match the heat flow through the TE legs. This equation and boundary condition can be expressed as follows:

$$\frac{d^2T}{dx^{*2}} = \phi(\sigma\epsilon' T^4 - C) \tag{13}$$

$$Q_H = -\frac{k_{SA}t_{SA}}{L_{SA}}\frac{dT}{dx^*}\Big|_{x^*=1} \tag{14}$$

with:

$$x^* = x/L_{SA} \tag{15}$$

$$\phi = \frac{L_{SA}^2}{k_{SA}t_{SA}} \tag{16}$$

$$C = \sigma\epsilon' T_C^4 + G\tau\alpha \tag{17}$$

where x* is a non-dimensional length along the solar absorber, ϕ determines the curvature of the temperature distribution in the absorber and C is a constant assuming the constitutive parameters are given. The significance of ϕ will be shown in later sections.

Once the temperature distribution has been solved with the boundary conditions met, electrical power output and efficiency can be solved for as before, where ΔT now depends on the temperature at the edge of the solar absorber.

C. Consideration of heat sink

In addition to the hot side of the TE leg seeing a reduced temperature from the theoretical maximum absorber temperature, the cold side will see an elevated temperature from the environmental temperature due to thermal resistance of the STEG heat sink. This also reduces performance, as the true ΔT that the TE elements are operating under is reduced. The cold side temperature of the TE leg is given by

$$T_{C,TE} = \frac{Q_C H_{HS}}{k_{HS} L_{HS}} + T_C \tag{18}$$

where the temperature increase (first term on right hand side of the equation) is the heat flow through the heat sink (heat flow into the TE leg less electrical power generated) multiplied by the thermal resistivity of the heat sink. In choosing the heat sink size, there is a balance between making the heat sink too small (as this will cause too considerable a cold side temperature increase, reducing power output) and too large (as this will have too much plan area dedicated to the heat sink, reducing efficiency).

D. Numerical Simulation

In addition to the mathematical models developed, we used the commercial software package COMSOL to run simulations for verification of the model's accuracy. Previous analysis considered only a one-dimensional temperature distribution in the absorber, whereas with COMSOL we simulated the more realistic two-dimensional distribution. COMSOL simulations also allowed the addition of more complicated features, such as finite electrical conductivity in the solar absorber and solar absorption and radiative losses in the TE legs, which were not included in the simplified mathematical models. In the COMSOL model, standard Fourier conduction was used for the absorber and heat sink sections (with

radiative boundary conditions at the free surfaces), while a TE model using conservation of charge and thermal energy which accounted for the Seebeck and Peltier effects was used for the TE domain. Power output was calculated by multiplying current through the TE leg and voltage drop across the device (TE leg and solar absorber).

E. Scaling considerations

With some manipulation of the temperature distribution equation (13) and boundary conditions it can be shown that there are a few parameters which determine performance regardless of scale. It is clear that ϕ is an important parameter which arises from the mathematics of the model. ϕ is the absorber length multiplied by its thermal resistance, which one would expect to have significant impact on the absorber temperature distribution. There is another important parameter that arises naturally from the mathematics as well. The temperature drop across the TE legs can be described by:

$$\Delta T = \frac{L_{TE}}{k'_{TE} t_{TE} PF} Q_H \tag{19}$$

where k'_{TE} is the effective thermal conductivity of the thermoelectric legs considering Fourier conduction as well as Peltier and Joule heating (whereas the standard thermal conductivity only accounts for Fourier conduction). The effective thermal conductivity is given in the ideal load matching case by:

$$\frac{k'_{TE}}{k_{TE}} = 1 + ZT_M \left(\frac{1 + \frac{T_H}{T_M}\sqrt{1 + ZT_M}}{\left(1 + \sqrt{1 + ZT_M}\right)^2} \right) \tag{20}$$

which can be derived by equating

$$Q_H = \Delta T \frac{k'_{TE} PF t_{TE}}{L_{TE}} \tag{21}$$

to the expression for Q_H given in Eq. (1). Substituting Q_H from Eq. (14) into Eq. (19) yields:

$$\Delta T = \frac{L_{TE}}{k'_{TE} t_{TE} PF} \frac{k_{SA} t_{SA}}{L_{SA}} \left(- \frac{dT}{dx^*} \Big|_1 \right) \tag{22}$$

Here the non-dimensional term preceding the temperature gradient is the ratio between the thermal resistance of the TE legs and the solar absorber, which will be designated γ', and can be expressed as follows:

$$\gamma' = \frac{L_{TE}}{L_{SA}} \frac{k_{SA} t_{SA}}{PF k'_{TE} t_{TE}} \tag{23}$$

It can be shown that if ϕ, defined by Eq. (16), and γ' are maintained, despite changing other parameters (thicknesses, packing fraction, and absorber conductivity), the non-dimensional temperature distribution for Eq. (13) and the associated boundary conditions are still met. Configurations with identical temperature distributions will have the same values for η_{ot} and η_{te}, and overall performance will only differ if η_{geom} changes. In the case of t_{SA} and t_{TE} being scaled equally (with ϕ and γ' held constant), it can be shown that η remains the same.

An important derived parameter is the product of ϕ and γ', which is the strongest determining factor of the hot side temperature. We will label this parameter β':

$$\beta' = \frac{L_{SA} L_{TE}}{PF k'_{TE} t_{TE}} \tag{24}$$

This is the product of solar absorber length and TE leg thermal resistance, with units of K m^2/W, so it makes sense that it would be related to temperature difference for a given solar insolation and that it

would have a significant impact on hot side temperature. This grouping can be related to the quantity $C_{th}L$ (geometric concentration ratio times TE leg length) that has been explored previously[22,23], with the main differences being the inclusion of k'_{TE} and that since this analysis includes temperature drop in the absorber, the hot side temperature is not only a function of β'.

It should be noted that because k'_{TE} is a function of temperature, some problems arise if one attempts to evaluate a configuration with a given β' or γ', since the hot side junction temperature is unknown, which adds unneeded iterative steps. k'/k is relatively constant for the range of temperatures with which we are concerned (less than 2% change for $ZT_M = 1$ from $T_H = 450$ K to 550 K or 177 °C to 277 °C). If k'/k is treated as constant, then k' and k can be interchanged in β' and γ', as their absolute values are somewhat arbitrary. Thus, the following expressions (note lack of k') are used for the remainder of the analysis:

$$\beta = \frac{L_{SA}L_{TE}}{PFk_{TE}t_{TE}} \tag{25}$$

$$\gamma = \frac{L_{TE}}{L_{SA}}\frac{k_{SA}t_{SA}}{PFk_{TE}t_{TE}} \tag{26}$$

It should be noted however that the treatment of exchanging k and k' is not necessarily acceptable for other thermoelectric materials or temperature ranges.

These parameters give more direct expressions for geometric and opto-thermal efficiencies (the expression for geometric efficiency assumes $L_{HS} = 0$):

$$\eta_{geom} = \frac{1}{1+\gamma\frac{PFk_{TE}t_{TE}}{k_{SA}t_{SA}}} \tag{27}$$

$$\eta_{ot} = \frac{-1}{\phi G}\frac{dT}{dx^*}\Big|_{x^*=1} \tag{28}$$

The TE leg efficiency is still a simple function of T_H and ZT_M (8).

III. RESULTS AND DISCUSSION

The table below shows the parameter values used for numerical simulations.

Table I: Parameters used in simulation

Parameter	Symbol	Value
Solar insolation	G	1000 W/m^2
Cold side and ambient temperature	T_C	300 K
Enclosure transmittance	T	0.95
Absorber effective absorptance	A	0.95
Absorber effective emmittance	ε'	0.075
Absober thermal conductivity	k_{SA}	400 W/m/K
Absorber electrical conductivity	$\sigma_{e,SA}$	6*10^7 S/m
TE dimensionless figure of merit	ZT_M	1
TE thermal conductivity	k_{TE}	1.6 W/m/K
TE leg packing fraction	PF	0.5
Heat sink thermal conductivity	k_{HS}	150 W/m/K

The solar insolation value is standard for AM 1.5G solar spectrum specifications[24]. Insolation affects the temperature distribution [Eqs. (13) (17)] and opto-thermal efficiency [Eq. (28)], with higher values leading to better overall performance. The transmittance value is taken as reasonable for a glass enclosure. The absorber properties are commercially achievable (the emittance takes into account losses from both the front and back sides), with thermal and electrical conductivity values typical for copper,

which would easily be used as a heat spreader beneath the selective surface. The dimensionless thermoelectric figure of merit is taken to be constant for simplicity, and is typical of bismuth telluride[25,26]. The TE thermal conductivity is given explicitly as it arises in determining η_{geom} (27). A conservative packing fraction is used, which also influences η_{geom} (lower packing fractions lead to better performance). The heat sink thermal conductivity value is typical of crystalline silicon, as the planar STEG was imagined to take advantage of MEMS fabrication techniques. As long as ϕ and γ remain constant, the thickness of the absorber and TE elements can be scaled without a loss in efficiency, and they were always taken to be the same thickness.

Parametric studies varying β and γ as defined by Eqs. (25) and (26) were performed using the property values provided in Table I. Results from these parametric studies are provided below, with a focus on values of β and γ which led to the highest efficiency given the property values used.

A. Isothermal absorber

In the isothermal absorber case, thermoelectric and opto-thermal efficiencies are solely a function of absorber temperature. While β was derived working through mathematics of the 1-D temperature distribution case, it is still relevant here, as geometry determines hot side temperature and β has a one-to-one mapping with the hot side temperature (as it is equivalent to $C_{th}L$ investigated previously[22,23]).

With the isothermal absorber approximation, the same value of β can be maintained while varying the relative lengths L_{SA} and L_{TE} in Eq. (25). This means that L_{SA} can be made arbitrarily large and L_{TE} can be made arbitrarily small, leading to a geometric efficiency of 1. Therefore in the isothermal absorber case, performance of the planar STEG is indiscernible from the performance of traditional STEG configurations. As an example, for a TE leg thickness of 500 nm and packing fraction of 0.5, if L_{SA} is set at 5 cm, the corresponding L_{TE} for optimal performance is about 4 μm, four orders of magnitude smaller. While this particular device would be almost impossible to fabricate, it demonstrates that in the

isothermal approximation TE leg plan area can be made negligibly small as long as contact resistance is ignored.

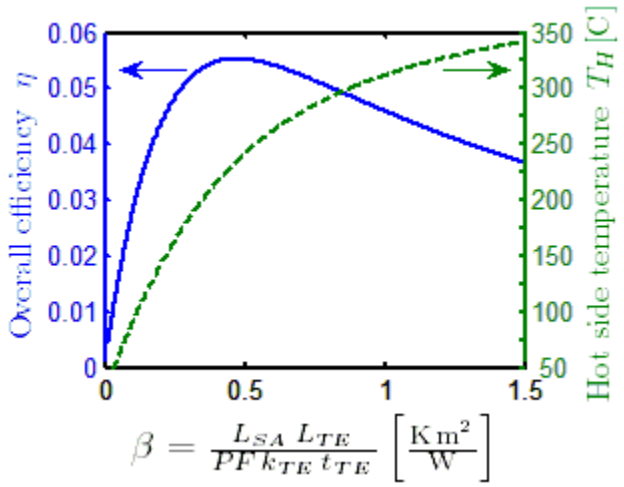

Figure 2. Efficiency (left axis, solid line) and absorber temperature (right axis, dashed line) for varying β in isothermal absorber approximation

Figure 2 shows hot side temperature and corresponding efficiency for a range of β. The maximum efficiency is slightly over 5.5% at a hot side temperature of 235 °C, which corresponds to a β of about 0.47 K m^2/W. As with previous work, higher temperatures lead to better thermoelectric efficiencies but worse opto-thermal efficiencies, resulting in an optimal hot side temperature[7]. Larger values of β lead to higher temperatures, so the optimal hot side temperature is achieved with a corresponding optimal β. This result provides a decent starting point for selecting β when finite absorber conduction is considered, as will be shown later.

B. 1-D Absorber temperature distribution

A noticeable drop in efficiency is observed when the temperature distribution within the absorber is accounted for. A typical temperature distribution is shown in Fig. 3, in this case for β = 0.45 K m^2/W and γ = 14.

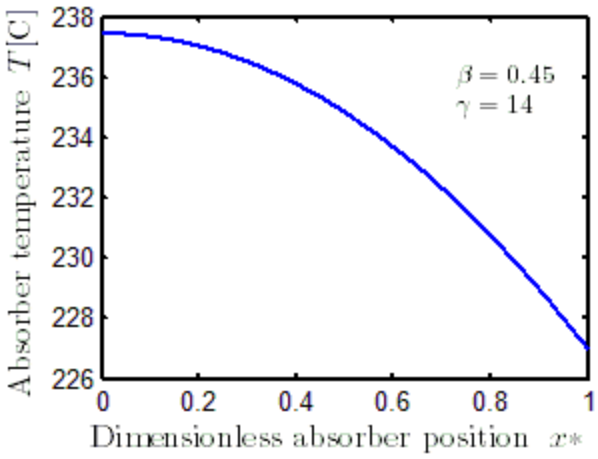

Figure 3. Temperature distribution along absorber for β = 0.45 and γ = 14

The temperature drop from the center of the absorber to the junction with the TE leg is about 11 °C . This temperature drop is responsible for the reduced efficiency, and adds some complexity to the device design. Efficiency is no longer solely a function of a uniform hot side temperature, but rather a function of both the parameters β and γ, which were defined earlier. β affects the overall absorber temperature, and γ affects the slope of the temperature distribution, which is demonstrated in Fig. 4.

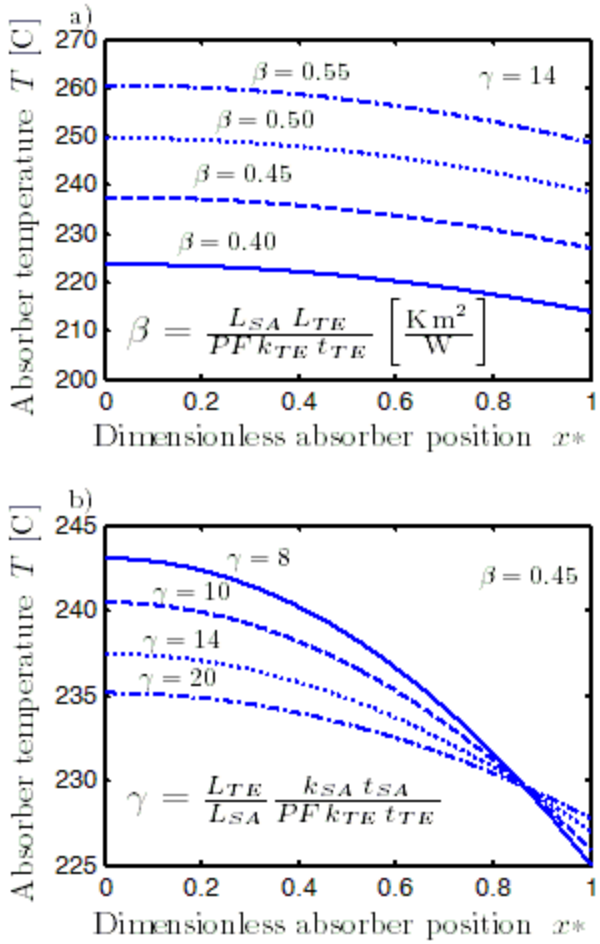

Figure 4. Temperature distributions in absorber for a) varying β with constant γ and b) varying γ with constant β

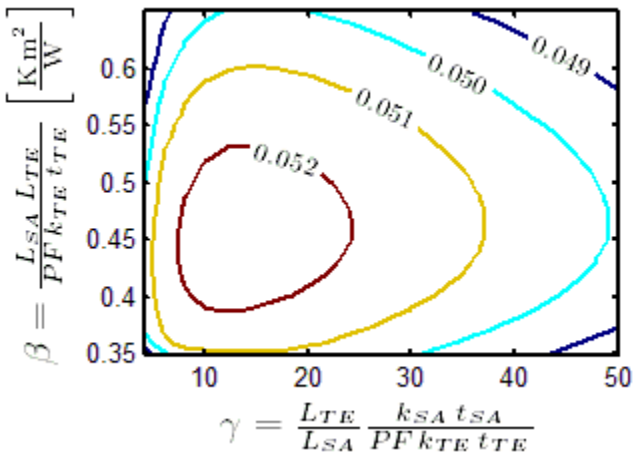

Figure 5. Efficiency contour plots for varying β and γ

It is important to find a suitable value of both β and γ to achieve a high efficiency. Figure 5 shows efficiency contours plotted against β and γ. The maximum efficiency in this case is about 5.25% with a β of 0.46 K m^2/W and a γ of 14. For an absorber and TE leg thickness of 500 nm with a packing fraction of 0.5, these values correspond to an absorber length of 2.6 mm and a TE leg length of 72 μm. Efficiency is very sensitive to β as this is the main determinant of absorber temperature, which heavily affects η_{te} and η_{ot}. There is also an optimal γ, which arises from the competition of two modes of efficiency loss. When γ is small, there is a large temperature drop in the absorber (operation is far from the isothermal absorber case), so the TE legs see a reduced temperature and η_{te} and η_{ot} are lowered. It is readily apparent that the lower ΔT will lead to a reduced η_{te}, but it is important to note that the lower ΔT also leads to a lower Q_H and therefore η_{ot}, which is contrary to the behavior of η_{ot} in the isothermal absorber case. When γ is large, the TE legs are relatively long, and η_{geom} is lowered.

The optimal value of β appears mostly constant near 0.45 K m^2/W, even for different packing fractions and absorber conductivities, however the optimal value of γ varies. Lower packing fractions result in better overall efficiency, because the reduced thermoelectric leg length minimizes the geometric efficiency loss from sunlight incident on non-absorber surfaces. However, the benefit predicted from the 1-D model will overstate reality, as it does not consider temperature gradients in the y-direction that would occur for low packing fractions (in later sections it will be shown that this is of negligible concern). It also ignores contact resistance, which would lead to a large performance reduction for very short TE legs in practice. Increasing absorber thermal conductivity naturally increases efficiency, as it drives operation closer to the isothermal absorber case.

It was found that while the optimal γ varied for different configurations, the product of the optimal γ and the length ratio L_{TE}/L_{SA}, given by $(L_{TE}/L_{SA})^2\ k_{SA}t_{SA}/(PFk_{TE}t_{TE})$, stayed approximately constant at 0.35 for the range of packing fractions and absorber conductivities investigated. This result is very useful, as it gives a strong starting point for which values of γ to consider when looking at a new device configuration (however it is important to note that this value will not hold for different TE properties). Keeping this

product constant accounts for the effect of changing parameters which maintain the same temperature distribution (i.e. γ and β held constant) and therefore η_{ot} and η_{te} but modify η_{geom}. When η_{geom} is improved (e.g. by decreased packing fraction or increased absorber conductivity), a higher γ value will be preferred for optimal performance, and this is accounted for by keeping $(L_{TE}/L_{SA})^2\, k_{SA}t_{SA}/(PFk_{TE}t_{TE})$ constant.

In some cases, the values of β and γ called for to maximize efficiency might not be feasible to achieve for structural or other reasons, as the proposed planar STEG involves very long, thin, suspended structures.

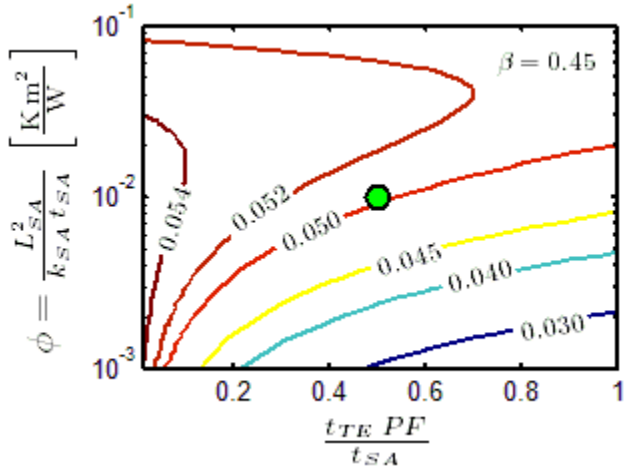

Figure 6. Efficiency with β = 0.45 K m^2/W for varying "manufacturing" parameters, with a sample operating point marked. Note ϕ is log scale

Figure 6 shows contour plots of efficiency for two parameters that would feasibly be limited from a manufacturing perspective. ϕ, if very large, corresponds to an extremely long and thin solar absorber, which might not be practically achievable. The other parameter, $t_{TE}PF/t_{SA}$, is a ratio of TE to solar absorber cross sectional area, which one would like to minimize, but in practice would be difficult as a small value corresponds to sparse, thin TE legs supporting a thick solar absorber. In this plot, β is held constant at 0.45 K m^2/W, so the efficiencies should be near optimal for the corresponding manufacturing parameters. A point for $t_{TE}PF/t_{SA}$ = 0.5, ϕ = 0.01 K m^2/W is marked in Fig. 6. This corresponds to a sample case using 10 μm thick TE elements and solar absorber with an absorber length of 6.3 mm, a TE

leg length of 0.6 mm and a packing fraction of 0.5, which would limit performance to around 5.0% efficiency.

It is also of interest to examine the effect of varying the effective emissivity (emissivity with back side losses considered) of the solar absorber. When emissivity is modified, the β corresponding to ideal performance changes, as changing the emissivity alters the balance between η_{ot} and η_{te}. Figure 7 shows the maximum efficiencies that can be achieved for different values of ε' and the corresponding value of β for a γ of 14.

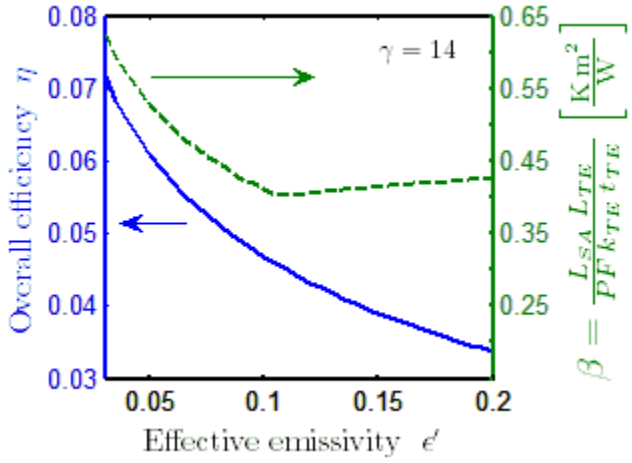

Figure 7 Efficiency (left axis, solid line) and β (right axis, dashed line) for varying ε'

For low emissivities, high values of β are preferred, since the lower emissivity allows for good opto-thermal efficiency even at high temperature. For high emissivities, β remains relatively constant, as it becomes more important to maintain an elevated temperature for a reasonable thermoelectric efficiency.

C. Consideration of heat sink

There is another drop in efficiency when some device area must be dedicated to a heat sink, in order to maintain the cold side temperature of the thermoelectric legs near the ambient temperature. In adding a heat sink, there are two competing factors which reduce efficiency. If the heat sink is large, there is a similar geometrical loss to having long thermoelectric legs, as any incident light striking the heat sink is

wasted. If the heat sink is small, the temperature rise from ambient to the cold side of the thermoelectric legs is large, which reduces ΔT and consequently generator efficiency.

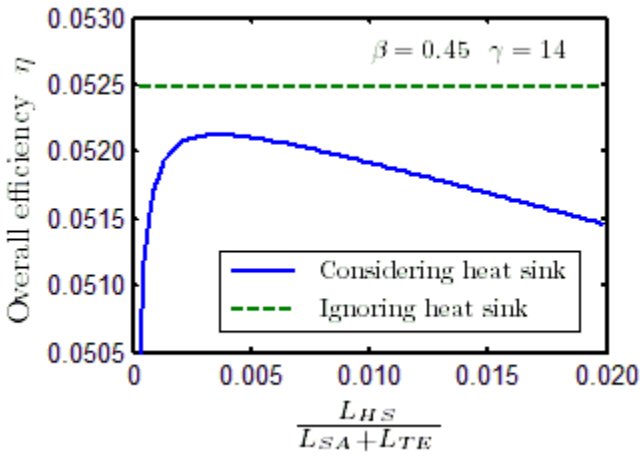

Figure 8. Efficiency for varying plan area dedicated to heat sink (solid line), compared to the ideal case (dashed line)

Figure 7 shows the device efficiency for various values of L_{HS} for a packing fraction of 0.5 with a β value of 0.45 K m^2/W and γ value of 14. The best performance when considering heat sink losses occurs with $L_{HS}/(L_{SA} + L_{TE})$ = 0.0035, and achieves an efficiency of 5.21%. This is a small drop from the value of 5.25% computed without consideration of the heat sink. For other β values and γ values the relative drop in efficiency is similar, and so consideration of heat sink effects on performance is not particularly important. The ideal value of $L_{HS}/(L_{SA} + L_{TE})$ is typical of other operating points as well. This suggests that in practice the heat sink width would be limited by fabrication and not by thermal considerations, as this analysis calls for absorbers millimeters long being supported by heat sinks which are micrometers wide.

D. Numerical Simulation Results

Results from COMSOL showed good agreement with results from the mathematical model, with typical errors less than 2%. This was found to be true for packing fractions down to 0.05, indicating that the 1-D assumption (no temperature distribution in the y direction) is an acceptable approximation for the

parameter values used in this study. When the effect of finite electrical conductivity (Joule heating) in the solar absorber was considered with copper properties, performance dropped a small amount (typically less than 0.1% absolute efficiency drop, indicating that the perfect electrical conduction approximation in the absorber is reasonable.

COMSOL simulations were also performed to evaluate the effect of a more realistic treatment of radiative absorption and emission in the thermoelectric legs. When the thermoelectric legs were modeled with an emissivity (and absorptivity) of 0.5 (typical of bismuth telluride), the drop in efficiency was on the order of 0.1% for large packing fractions (0.8) and almost negligible for low packing fractions (0.2). With the consideration of radiation in the TE legs, there was also a preference for lower values of γ, so optimal performance occurred with slightly smaller TE leg lengths.

IV. CONCLUSION

A mathematical model was developed to investigate the performance of a novel configuration for STEGs. In the ideal case, using characteristic material properties, the planar STEG has performance virtually identical to traditional STEG configurations. With the added considerations of temperature drop in the absorber and area taken up by a heat sink, the efficiency of the device drops slightly. This is in agreement with results from COMSOL simulations of the device. Potential advantages in manufacturing thin-film STEGs make it a very appealing option, as the loss in efficiency from switching to this configuration is minimal.

ACKNOWLEDGEMENTS

This material is based upon work supported as part of the Solid State Solar-Thermal Energy Conversion Center (S3TEC), an Energy Frontier Research Center funded by the U. S. Department of Energy, Office of Science, Office of Basic Energy Sciences under Award Number: DE-FG02-09ER46577.

REFERENCES

[1] E. Weston, U.S. Patent 389,124 (September 4, 1888).

[2] M. Telkes, J. Appl. Phys. 25, 765 (1954).

[3] H. J. Goldsmid, *Applications of Thermoelectricity* (Methuen, London, 1960).

[4] H. J. Goldsmid, J. E. Giutronich, and M. M. Kaila, Sol. Energy 24, 435 (1980).

[5] S. A. Omer and D. G. Infield, Sol. Energ. Mat. Sol. C. 53, 67 (1998).

[6] R. Amatya and R. J. Ram, J. Electron. Mater. 39, 1735 (2010).

[7] D. Kraemer, B. Poudel, H. P. Feng, J. C. Caylor, B. Yu, X. Yan, Y. Ma, X. W. Wang, D. Wang, A. Muto, K. McEnaney, M. Chiesa, Z. F. Ren, and G. Chen, Nat. Mater. 10, 532 (2011).

[8] L. L. Baranowski, G. J Snyder, and E. S. Toberer, Energy Environ. Sco. 5, 9055 (2012).

[9] K. McEnaney, D. Kraemer, Z. F. Ren, and G. Chen, J. Appl. Phys. 110, 074502 (2011).

[10] G. J. Snyder and E. S. Toberer, Nat. Mater. 7, 105 (2008).

[11] M. Zebarjadi, K. Esfarjani, M. S. Dresselhaus, Z. F. Ren, and G. Chen, Energy Environ. Sci. 5, 5147 (2012).

[12] H. Böttner, G. Chen, and R. Venkatasubramanian, MRS Bull. 31, 211 (2006).

[13] J. Tang, H. Wang, D. H. Lee, M. Fardy, Z. Huo, T. Russell, and P. Yang, Nano Lett. 10, 4279 (2010).

[14] R. Venkatasubramanian, E. Siivola, T. Colpitts, and B. O'Quinn, Nature 413, 597 (2001).

[15] F. Völklein, M. Blumers, and L. Schmitt, Int. Conf. Thermoelect. 18, 285 (1999).

[16] J. Nurnus, H. Bottner, C. Kunzel, U. Vetter, A. Lambrecht, J. Schumann, F Völklein, Int. Conf. Thermoelect. 21, 523 (2002).

[17] M. A. Green, J. Mater. Sci. Mater. El. 18, S15 (2007).

[18] R. Yang, G. Chen, G. J. Snyder, and J. P. Fleurial, J. Appl. Phys. 95, 8226 (2004).

[19] G. Min, D. M. Rowe, Solid-State Electron. 43, 923 (1999).

[20] G. J. Snyder, J. R. Lim, C. K. Huang, and J. P. Fleurial, Nat. Mater. 2, 528 (2003).

[21] M. Mizoshiri, M. Mikami, K. Ozaki, and K. Kobayashi, J. Electron. Mater. 41, 1713 (2012).

[22] G. Chen, J. Appl. Phys. 109, 104908 (2011).

[23] D. Kraemer, K. McEnaney, M. Chiesa, and G. Chen, Sol. Energy 86, 1338 (2012).

[24] "*ASTM G173-03(2008) Standard Tables for Reference Solar Spectral Irradiances: Direct Normal and Hemispherical on* 37° *Tilted Surface"* (ASTM International, West Conshohocken, Pennsylvania, USA, 2008), http://www.astm.org.

[25] W. S. Liu, Q. Zhang, Y. Lan, S. Chen, X. Yan, Q. Zhang, H. Wang, D. Wang, G. Chen, and Z. Ren, Adv. Energy Mater. 1, 577 (2011).

[26] X. Tang, W. Xie, H. Li, W. Zhao, Q. Zhang, and M. Niino, Appl. Phys. Lett. 90, 012102 (2007).